Article

Harmless Treatment of High Arsenic Tin Tailings and Environmental Durability Assessment

Weiwei Zhao [1], Zhengfu Zhang [1,*], Hui Yang [1], Xian Zhou [1,2], Jinsong Wang [1] and Chengping Li [1]

[1] Faculty of Materials Science and Engineering, Kunming University of Science and Technology, Kunming 650093, China

[2] Kunming Metallurgical Research Institute Co., Ltd., Kunming 650031, China

* Correspondence: zhang-zhengfu@163.com

Abstract: The treatment of arsenic (As) in tin tailings (TT) has been an urgent environmental problem, and stabilization/solidification (S/S) treatment is considered an effective technology to eliminate contamination of As. In this study, we developed a low-carbon and low-alkalinity material to S/S of As, and the results showed that the leaching concentration of As after treatment was lower than the Chinese soil environmental quality standard (0.1 mg/L). Based on a series of characterization tests, we found that OH^- promoted the dissolution of As(III)-S, Fe-As(V), and amorphous As(III)-O species and formed Ca-As(III) and Ca-(V) species with Ca^{2+}. Simultaneously, hydration produces calcium silicate hydrate (C-S-H) gel and ettringite by the form of adsorption and ion exchange to achieve S/S of As. We also assessed the durability of this material to acidity and temperature, and showed that the leaching concentration of As was below 0.1 mg/L at pH = 1–5 and temperature 20–60 °C. The method proposed in this study, S/S of As, has excellent effect and environmental durability, providing a new solution for harmless treatment of TT and its practical application.

Keywords: arsenic; environmental durability; mechanism of stabilization/solidification; tin tailings (TT)

1. Introduction

The rapid development of industry has greatly improved people's material life; simultaneously, the awareness of environmental protection has gradually increased. Especially in the development and utilization of mineral resources, a huge amount of low-utilization tailings are often produced, which not only take massive valuable land resources but also the harmful elements such as arsenic (As) in the tailings will spread to the surrounding soil and water sources over time, which will eventually endanger human life and health through the action of the food chain [1,2].

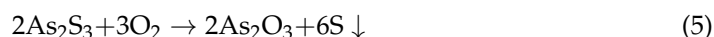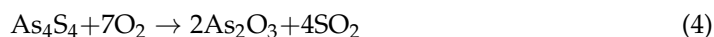As is a metallic element that is widely distributed in the Earth's crust and can be As^{3-} (arsine), As^0 (arsenic monomers), As^{3+} (arsenite), and As^{5+} (arsenate) valence states. As monomers exist in three isotopes: gray As, yellow As, and black As [3]. Gray As is the most common As monomer, a bilayer structure, which is composed of many interlocked vertical six-membered rings with weak bonding between the layers [4,5]. The As^{3+} form and the As^{5+} form are the most common valence states, and inorganic compounds consisting of As^{3+} are more toxic than As^{5+} [6]. Currently, the use of As is limited and is commonly used as wood preservation, pesticides, etc. [7]. As in minerals is mainly in the form of sulfides such as arsenopyrite (FeAsS) [8], realgar (As_4S_4) [9], and orpiment (As_2S_3) [10], and these compounds are often found in tailings and are relatively stable in strong alkaline and reducing environments [11]. Under the action of natural weathering conditions, As will be released into the environment [12]. The process of FeAsS oxidation reaction is shown as follows:

$$4FeAsS + 11O_2 + 6H_2O \rightarrow 4Fe^{2+} + 4H_3AsO_3 + 4SO_4^{2-} \tag{1}$$

$$2H_3AsO_3 + O_2 \rightarrow 2H_2AsO_4^- + 2H^+ \tag{2}$$

$$4Fe^{2+} + O_2 + 4H^+ \rightarrow 4Fe^{3+} + 2H_2O \tag{3}$$
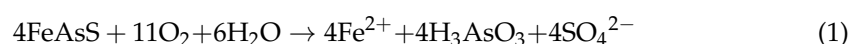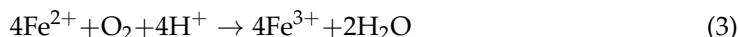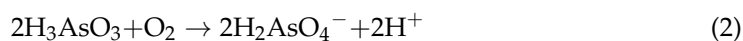
As_4S_4 is easily converted to As_2O_3 under oxidation conditions. The process of As_2S_3 oxidation reaction is shown as follows:

$$As_4S_4 + 7O_2 \rightarrow 2As_2O_3 + 4SO_2 \tag{4}$$

$$2As_2S_3 + 3O_2 \rightarrow 2As_2O_3 + 6S \downarrow \tag{5}$$

$$As_2O_3 + 3H_2O \rightarrow 2H_3AsO_3 \tag{6}$$

Under different weathering conditions, the oxidation products of As are different, but most of them are produced in the form of arsenate. Oxidation of As-S minerals such as FeAsS will result in an increase in the leaching of As from the tailings, which poses a serious hazard to the surrounding environment [13]. Studies have shown that the reaction of iron and calcium salts with arsenate ions produces the corresponding precipitates, which can effectively reduce the leaching of As from tailings [14–16]. However, there are some differences in the composition and types of As-containing minerals in different types of tailings or the same type of tailings from different regions [9]. Current studies have generally focused on the study of As in gold tailings, but little attention has been paid to the species and transformation processes of As in tin tailings (TT), and different species of As may have different effects on the immobilization of As in tailings.

Stabilization/solidification (S/S) is a technique which can eliminate or reduce the hazards of solid waste by using a binder to physically encapsulate and chemically immobilize the hazardous components in the solid waste [17,18]. It has a series of advantages, such as the ability to control the content of As quickly, low treatment cost, and simple process operation [19]. Ordinary Portland cement (OPC) is a typical binder, and the calcium silicate hydrate (C-S-H) gel generated by the OPC hydration process can effectively adsorb or ion exchange with As. Furthermore, the alkaline environment is also favorable to promote the generation of As precipitation [20]. However, the heavy use of OPC increases the treatment cost, energy consumption, and CO_2 emissions [21]. Therefore, it is necessary to develop an efficient and environmentally friendly solution for S/S of As. This article is based on adding no alkali activator or any foreign additives, using low OPC clinker and TT for S/S of As; calcium hydroxide ($Ca(OH)_2$) generated by OPC hydration can also activate TT [14]. Theoretically, it can maintain a certain strength and immobilization efficiency, and can greatly reduce the price and environment cost. In addition, $3CaO \cdot Al_2O_3$ (C_3A) in OPC will generate ettringite in the presence of gypsum ($CaSO_4 \cdot 2H_2O$) and $Ca(OH)_2$ [22]. Ettringite is considered to be an ideal substance for S/S of As, and it mainly undergoes chemical substitution with As [23]. This study also comprehensively assesses the environmental durability to S/S of As. In natural environments, pH and temperature are important factors affecting the leaching of As in the encapsulator [24,25]. Under acidic conditions, the As precipitates in the encapsulator may be dissolved and re-released into the environment. The hydration products C-S-H gel and ettringite will also be affected [26,27]. There is a certain relationship between temperature and microstructure changes in the encapsulator, which would lead to a decrease in the performance for S/S of As [27].

In this work, we analyzed TT and investigated the compressive strength and leach property of As in the encapsulator at different OPC additions by the technology of S/S. The main species and stabilization mechanism of As in the encapsulator was also determined by various characterization tests. Durability studies were also performed for the encapsulator with different pH and temperature.

2. Materials and Methods

2.1. Materials and Experimental Procedure

The TT used in this study come from Gejiu, Yunnan Province, China, which enjoys the reputation of the word capital of tin—it has a very long mining history. There are a lot of

harmful elements such as As in the TT. OPC was purchased from a factory in Zhengzhou City, Henan Province. The chemical compositions of OPC and TT were measured by X-ray fluorescence analysis (XRF), as shown in Table 1. In order to explore the effect on S/S of As, OPC and ground TT were mixed in different proportions according to the scheme in Table 2. The percentage of OPC was increased from 25 wt% to 75 wt%, and the water–binder ratio was adjusted to 0.28 according to the actual situation. Then, the mixed slurry was poured into a 40 mm × 40 mm × 40 mm plastic mold and placed at room temperature for 24 h. Then, the hardened slurry was demolded, cured to the corresponding age in a curing box at 90% humidity and 20 °C, and its compressive strength and leaching concentration of As tested. The chemical reagents nitric acid (HNO_3), glacial acetic acid (CH_3COOH), and sodium hydroxide (NaOH) used in this experiment were obtained from Shanghai Sinopharm Chemical Reagent Factory.

Table 1. Chemical compositions of OPC and TT (wt%).

Material	Al_2O_3	CaO	Fe_2O_3	K_2O	MgO	P_2O_5	SiO_2	SO_3	LOI
OPC	7.1	41.3	6.2	0.3	2.8	0.09	24.5	0.05	17.66
TT	6.2	28.5	16.4	1.1	0.08	0.06	31.7	2.4	13.56

LOI: Loss on ignition.

Table 2. Mixture formulations (wt%) for OPC and TT.

| Sample	Mixture Ratio (wt%)		Water Cement Ratio (W/C)
	TT	OPC	
CM1	75	25	
CM2	66.7	33.3	
CM3	50	50	0.28
CM4	33.3	66.7	
CM5	25	75	

2.2. Leaching Tests

The leaching test was performed according to the TCLP Standard [28], and the ratio of sample to leachate was kept at 1 kg/20 L. An aqueous solution of acetic acid with pH maintained at 2.88 ± 0.05 was used as the leachate, and the pH was adjusted with HNO_3 or NaOH. The solution was turned over at 30 rmp for 18 h at room temperature, and the pH of the solution after flipping was measured. The leachate was filtered through a 0.45 μm microporous membrane. Finally, the As leaching concentration was measured after acidifying with HNO_3 to pH < 2. To better evaluate the environmental durability of the encapsulator, the samples were immersed in acidic solutions of pH 0–5 to investigate the effect of pH on the leachability of As, while the same samples were immersed in solutions with temperature gradients of 20–60 °C. As leaching concentrations were tested after 7 days.

2.3. Analysis and Characterization

A pH meter (Mettler FB28, benchtop acidity meter) was used to measure the weak alkalinity of the TT, pH = 8.64. The compressive strength of the samples at the corresponding age was measured by a digital pressure tester. The concentration of As in the solution after leaching the encapsulator was measured by inductively coupled plasma emission spectrometry (ICP-OES). Chemical speciation of As in TT obtained by European Community Bureau of Reference (BCR) sequential extraction analysis is presented in Figure 1, in which As is divided into acid soluble/exchangeable (F1), reducible-fraction (F2), oxidizable-fraction (F3), and residual (R) [29]. The physical phase composition of OPC, TT, and samples was determined by X-ray diffraction (XRD), setting the scan range to 5–70° and scan speed to 5°/min. Analysis of sample morphology using Scanning electron microscopy (SEM, Hitachi Regulus8100). The elemental composition of the sample was measured and analyzed by Energy dispersive spectroscopy (EDS). The functional groups

Int. J. Environ. Res. Public Health **2022**, *19*, 11247

4 of 14

of the samples were measured by Fourier transform infrared spectroscopy (FTIR) with a set scan range of 4000–400 cm^{-1}, a resolution of 4 cm^{-1}, and 16 scans. The samples were tested by X-ray photoelectron spectroscopy (XPS, Thermo Fisher ESCALAB XI+) to analyze the binding energy, valence, and chemical shifts of the relevant As elements.
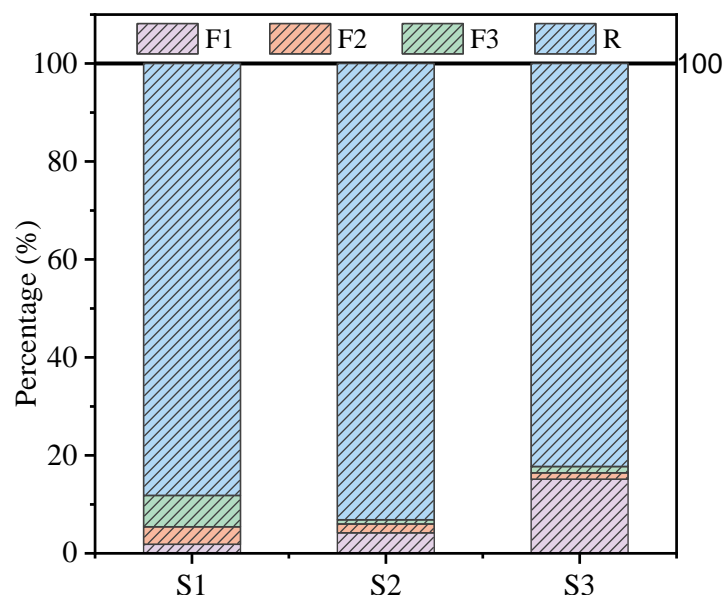

Figure 1. The percentage of each fraction of As in TT extracted by the BCR sequential extraction procedure.

3. Results and Discussion
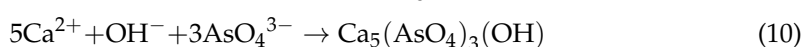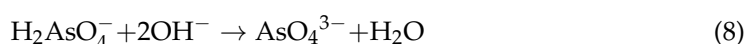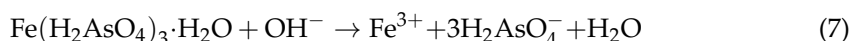
3.1. X-ray Diffraction Analysis of TT and Sample

Figure 2a is the XRD spectra of TT, and the main minerals are calcite ($CaCO_3$), quartz (SiO_2), fluorite (CaF_2), and hedenbergite ($CaFe [2Si_2O_6]$). In addition, orpiment (As_2S_3, PDF#24-0075) and iron hydrogen arsenate hydrate (PDF#26-0784) were also detected. $Fe(H_2AsO_4)_3 \cdot H_2O$ is the phase formed by the oxidation of As and sulfur minerals in TT. Other phases, such as sekaninaite ($Fe_2Al_4Si_5O_{18}$) and phlogopite ($KMg_3(Si_3Al)O_{10}(OH)_2$) also correspond to the major elements in the chemical composition.
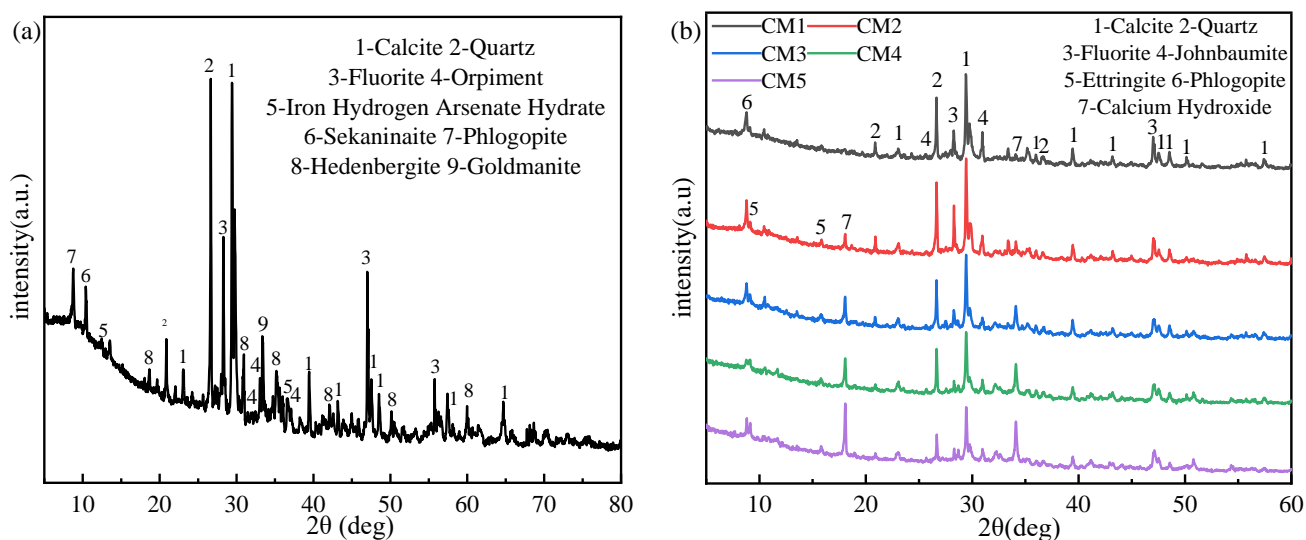

Figure 2. XRD spectra of tin tailing (**a**) and sample of CM1 to CM5 (**b**).

Int. J. Environ. Res. Public Health **2022**, *19*, 11247

5 of 14

In order to understand the change process of As species after curing, the phase composition of the sample was analyzed by XRD, as shown in Figure 2b. Except for the presence of calcite ($CaCO_3$, PDF#47-1743), quartz (SiO_2, PDF#46-1045) and fluorite (CaF_2, PDF#35-0816) phases in the TT, obviously, the mineral species of As changed before and after the S/S treatment with the appearance of johnbaumite ($Ca_5(AsO_4)_3(OH)$, PDF#33-0265), which indicates that the As species in the TT underwent chemical reactions during solidification. $Fe(H_2AsO4)_3 \cdot H_2O$ from TT released Fe^{3+} and H_2AsO^{4-} in water, and produced $Ca_5(AsO4)_3(OH)$ in the presence of Ca^{2+} and OH^-, the transformation process of As is shown below:

$$Fe(H_2AsO_4)_3 \cdot H_2O + OH^- \rightarrow Fe^{3+} + 3H_2AsO_4^- + H_2O \tag{7}$$

$$H_2AsO_4^- + 2OH^- \rightarrow AsO_4{}^{3-} + H_2O \tag{8}$$

$$Fe^{3+} + 3OH^- \rightarrow Fe(OH)_3 \tag{9}$$

$$5Ca^{2+} + OH^- + 3AsO_4{}^{3-} \rightarrow Ca_5(AsO_4)_3(OH) \tag{10}$$

It was shown that the diffraction peaks around 30° are related to the formation of C-S-H gels which are usually in an amorphous state, so that no distinct characteristic peaks are observed [30]. A distinct calcium hydroxide ($Ca(OH)_2$, PDF#44-1481) diffraction peak can also be observed, which is due to the reaction of CaO in the cement with water to generate $Ca(OH)_2$ [31]. With the increase of OPC content, the amount of $Ca(OH)_2$ generated increases, and the intensity of the diffraction peak increases, which is also consistent with the increase of pH value of the leaching solution in Figure 3b. The appearance of ettringite is due to the chemical reaction between C_3A with a small amount of gypsum ($CaSO_4 \cdot 2H_2O$) doped in the mixture, which is beneficial to the S/S of As. The peak intensity of ettringite increases with increasing OPC content, indicating that more ettringite was generated, which also explains the increasing trend of compressive strength. $Ca(OH)_2$ can also be used as an alkali activator to activate the TT [32], and with the increase of OPC content, ettringite has a tendency to gradually increase.
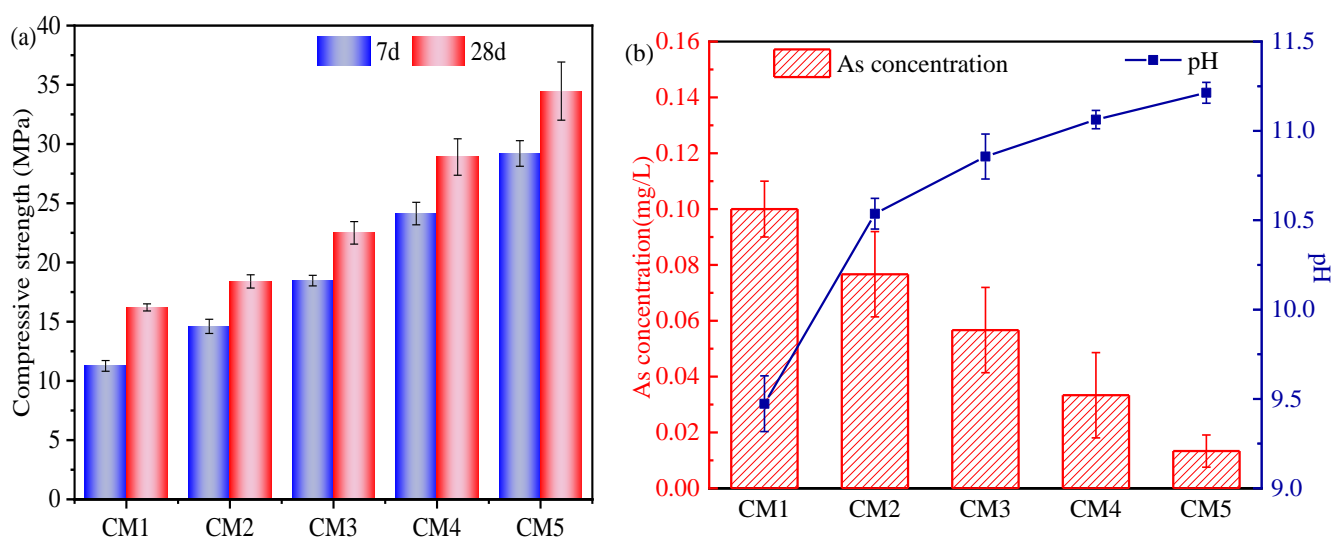
Figure 3. (**a**) Compressive strength of samples (CM1-CM5) after 7 and 28 days in a curing box at 90% humidity and 20 °C, (**b**) the leaching concentration of As and pH after curing 28 days.

3.2. Compressive Strength and Leaching Test

As shown in Figure 3a, the 7-day and 28-day compressive strengths of sample showed a sequential increase with the increase of cement content. At the highest content of TT, the compressive strengths of sample for 7 days and 28 days respectively were 11.3 MPa and 16.2 MPa, and the presence of less active substances in TT was not conducive to the

Int. J. Environ. Res. Public Health **2022**, *19*, 11247

6 of 14

development of compressive strength. The compressive strengths of sample for 7 days and 28 days were 28.9 MPa and 34.7 MPa when the TT content was the lowest. The increase in cement content promoted the formation of more C-S-H gels. These C-S-H gel phases were filled in the voids between the hydration products, which increases the structure compactness and greatly improves the compressive strength [33,34]. The formation of ettringite is beneficial to improve the early compressive strength [35]. In addition, ettringite also has a certain degree of swelling, which can reduce the porosity of the encapsulator and further improve the compactness of the structure [36].

The trend of As leaching concentration obtained from the experiment is shown in Figure 3b, where the concentration of As in the solution is inversely proportional to the content of TT. With the decrease of TT, the leaching concentration of As decreased from 0.1 mg/L to 0.01 mg/L, and the pH value increased from 9.47 to 11.21. The presence of many alkaline substances in the cement, which generated OH^- during the hydration process, explains the increase of the pH value of the leachate after 28 days, and facilitated the formation of Ca-As compound precipitation [37], thus proving the reason for the decrease of As leaching concentration. In addition, OPC hydration products such as C-S-H gels have adsorption effects on As, and the hydroxide colloids formed by Fe^{2+} and Fe^{3+} in alkaline environment can adsorb different forms of As-containing compounds on the surface or encapsulate them in the colloids [38].

3.3. Fourier Transform Infrared Spectroscopy Analysis

Figure 4 shows the FTIR spectra of CM1–CM5 with similar trends for all the curves. The functional groups corresponding to the FTIR absorption peaks are summarized in Table 3. The peak at 3426.9 cm^{-1} is due to the -OH stretching vibration from water in the free state of the sample. The peak at 1632.5 cm^{-1} is H-O-H bending vibration, indicating the presence of C-S-H. The peak at 1414.8 cm^{-1} is the stretching vibration caused by the O-C-O of the carbonate. The peaks at 1112.7 cm^{-1} and 713.2 cm^{-1} are the v3 and v4 vibrations of SO_4^{2-}, which implies the presence of ettringite. The peaks at 1006.7 cm^{-1} and 518.4 cm^{-1} are the v3 and v4 vibrations of SiO_4^{2-}. The peak at 875 cm^{-1} is attributed to the As-O stretching vibration, which corresponds to the formation of arsenic–oxygen compounds in Figure 2b. It is further verified that As in TT exists in the form of precipitation [39,40]. The peak at 464 cm^{-1} indicates the Si-O bending vibration.
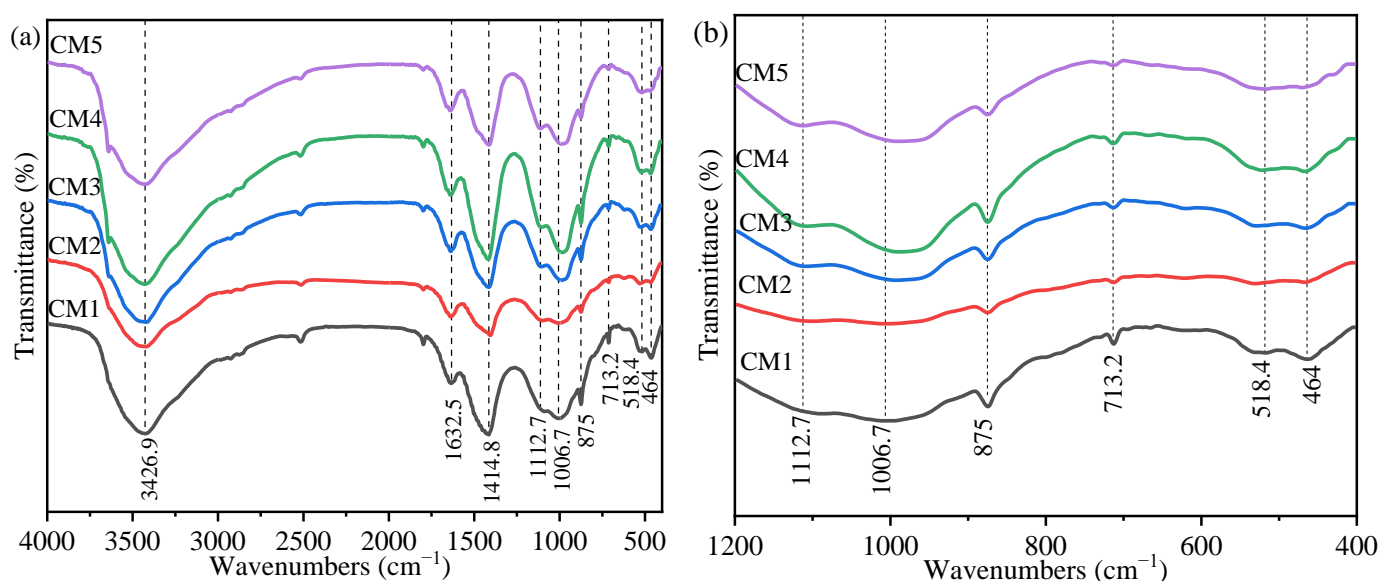

Figure 4. FTIR spectra of sample CM1 to CM5 (**a,b**).

Table 3. Peaks detected by FTIR spectroscopy and the corresponding functional groups.
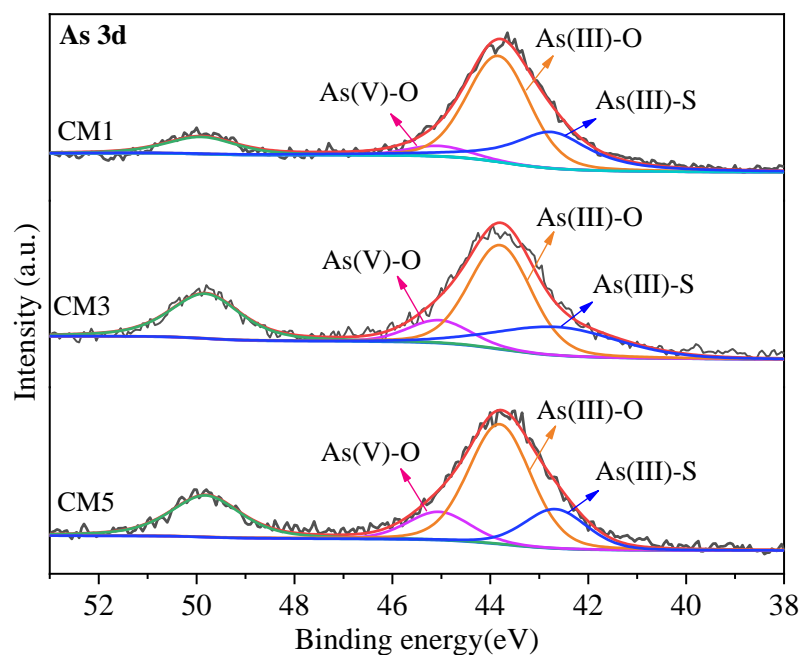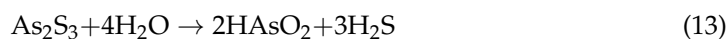
Wavenumbers (cm^{-1})	Functional Group	Types of Vibration	Reference
3426.9 cm^{-1}	Free H_2O	stretching vibration	[30]
1632.5 cm^{-1}	H_2O in C-S-H	bending vibration	[41]
1414.8 cm^{-1}	O-C-O	stretching vibration	[42]
1112.7 cm^{-1}	SO_4^{2-}	v3 vibrations	[43]
1006.7 cm^{-1}	SiO_4^{2-}	v3 vibrations	[44]
875.0 cm^{-1}	As-O	stretching vibration	[45,46]
713.2 cm^{-1}	SO_4^{2-}	v4 vibrations	[16]
518.4 cm^{-1}	SiO_4^{2-}	v4 vibrations	[47]
464.0 cm^{-1}	Si-O	bending vibration	[48]

*3.4. X-ray Photoelectron Spectroscopy Analysis*

From the XPS spectrum of Figure 5, it was observed that As(III)-O dominates in the sample, exists in an amorphous state, and forms a precipitate with Ca^{2+}, the transformation process of As is shown below:

$$2H_3AsO_3 + 3OH^- \rightarrow AsO_3^{3-} + 3H_2O \tag{11}$$

$$3Ca^{2+} + 2AsO_3^{3-} \rightarrow Ca_3(AsO_3)_2 \tag{12}$$
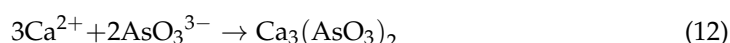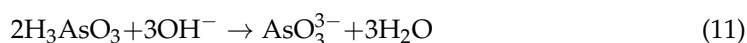
As in TT is mainly present in the form of As_2S_3 and FeAsS species in Figure 2. The presence of As(V)-O, As(III)-O, and As(III)-S can also be observed in the XPS spectra of the treated TT in Figure 5. During the process from CM1 to CM5, As(III)-S decreased from 32.5% to 21.0% and As(V)-O increased from 6.1% to 15.1%, which indicates that As_2S_3 underwent dissolution and finally converted to As(V), and the oxidation process was very slow [9]. The percentage of As(III)-O was also changing, indicating that oxidation of As_2S_3 first formed As(III)-O and then further converted to As(V)-O. Although the solubility of As_2S_3 in water is small, the equation for the hydrolysis is as follows:

Figure 5. XPS spectra of CM1, CM3, and CM5 (**As 3d**).

$$As_2S_3 + 4H_2O \rightarrow 2HAsO_2 + 3H_2S \tag{13}$$

Int. J. Environ. Res. Public Health **2022**, *19*, 11247

8 of 14

Both $HAsO_2$ and H_2S react with alkali, and the reaction equations are as follows:

$$HAsO_2 + OH^- \rightarrow AsO_2^- + H_2O \tag{14}$$

$$H_2S + 2OH^- \rightarrow S^{2-} + 2H_2O \tag{15}$$
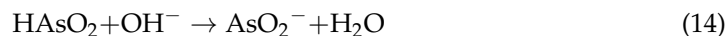
In the presence of O_2, the oxidation Equation (14) of arsenite is as follows:

$$2AsO_2^- + O_2 + 4OH^- \rightarrow 2AsO_4^{3-} + 2H_2O \tag{16}$$
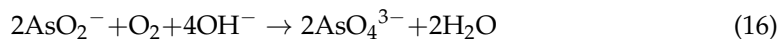
The XPS spectra show that the As species are dominated by As(III)-O. In addition to As_2S_3, other As sulfides and As_2O_3 in the tailings can be converted to arsenite during the synthesis process [49].

3.5. SEM-EDS Analysis

The presence of many white irregular amorphous C-S-H gels in Figure 6b is considered to be the main product of cement hydration; it is capable of S/S of As by physical adsorption, interlayer symbiosis, and ion exchange [50]. In addition, some needle-like crystal organization is typical for the shape of ettringite; it has a strong heavy metal immobilization ability, and anionic groups such as arsenate ions are able to ion exchange with SO_4^{2-} in ettringite for stabilization [31]. EDS in Figure 6c results show the presence of O, As, Ca, Si, Al, and Fe elements, indicating that As combines with Ca and Fe to produce the corresponding precipitates. Element S was found in Figure 6d, indicating that a portion of arsenic sulfide was still present and was not involved in the reaction, which is consistent with the results in Figure 5.
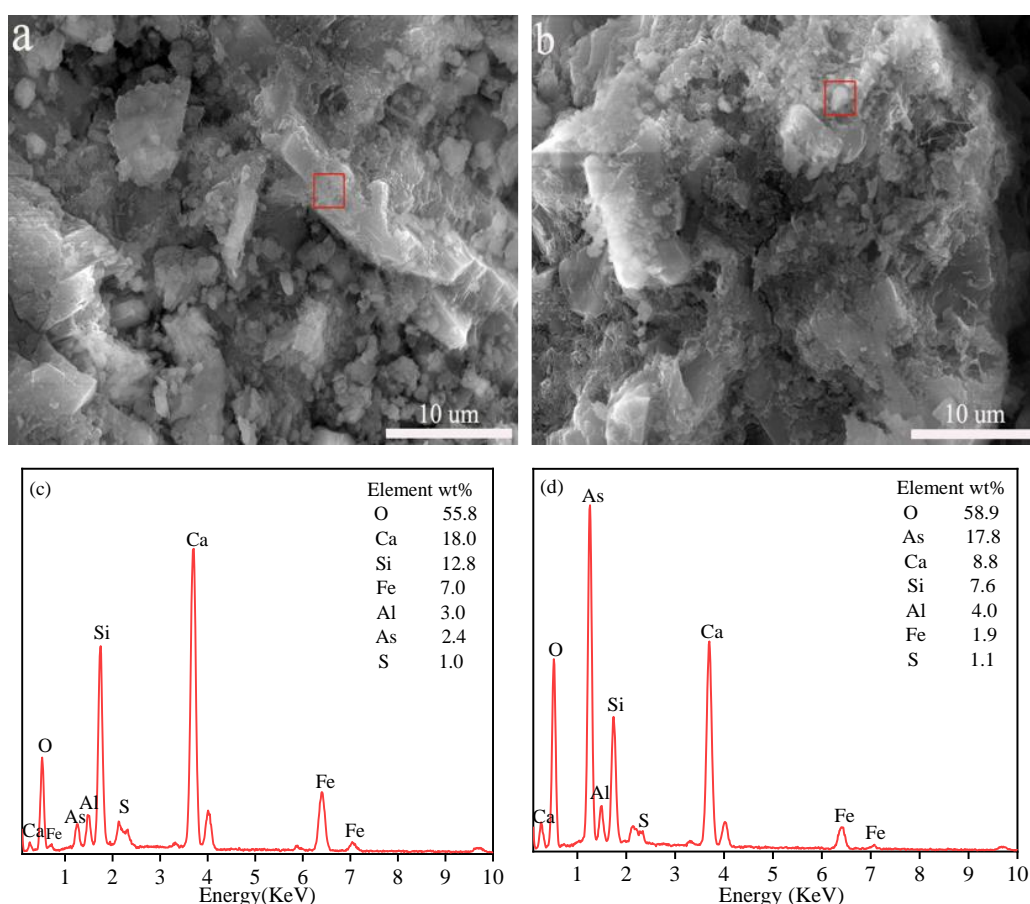
**Figure 6.** SEM images: (**a**) CM1 (**b**) CM5; and EDS analyses of elements composition: (**c**) CM1 (**d**) CM5.

3.6. Environmental Durability Assessment

The environmental durability assessment is to study the influence of external factors on the performance of S/S of As. This experiment mainly simulated the influence of two important factors, pH and temperature of acidic conditions, and to study their effects on the leaching behavior of As.

3.6.1. Effect of pH on the Leaching Behavior of As

The cured samples were dipped into the acid solution at a ratio of 1:10 (g/mL), the different solutions of pH 0–5 adjusted with HNO_3, and the leaching concentration of As was tested after 7 days. The results are shown in Figure 7a, the leaching concentration of As gradually decreased with the increase of pH, the concentration of As decreased from 1056.67 µg/L to 32.76 µg/L when the pH was between 0 and 1, and then the concentration of As showed a slow downward trend and finally dropped to 9.65 µg/L. The study showed that the release of As from the tailings was favorable under acidic environment. Especially in the strong acidic environment with pH = 0, the stability of As-S, Fe-As, and Ca-As species in the TT will substantially reduce [26,51]. Moreover, the structure of C-S-H and ettringite will be destroyed, leading to an increase of As leaching.
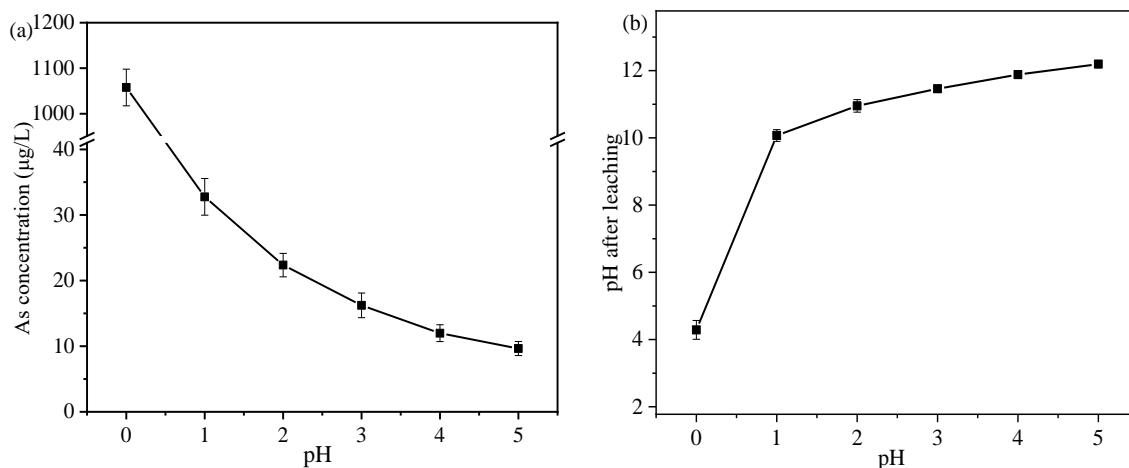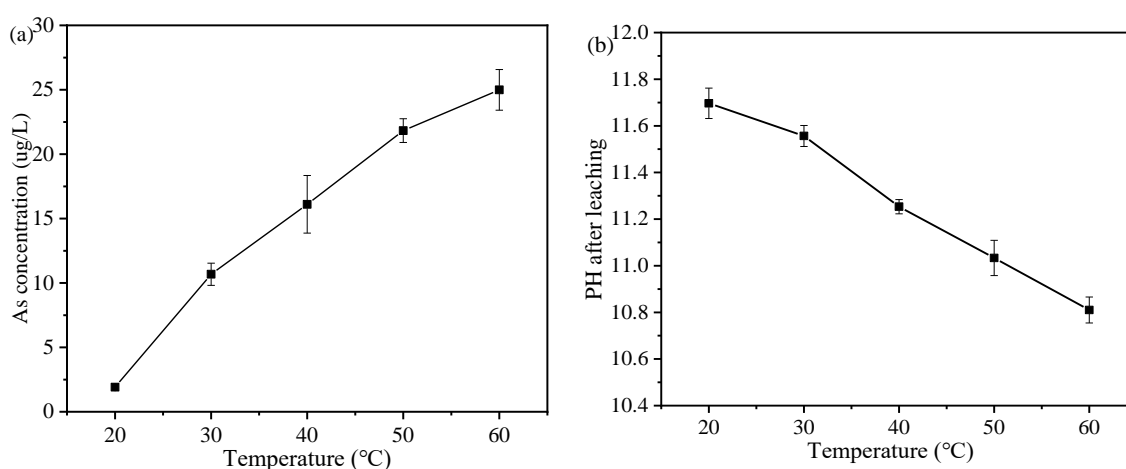

Figure 7. (**a**) The influence of different pH on the leaching concentration of As, (**b**) the change of pH after leaching.

Due to the presence of many alkaline substances in the encapsulator, mainly $Ca(OH)_2$ released OH^- to the solution, leading to an increase of pH in Figure 7b. In a solution with an initial pH of 0, the OH^- released by the encapsulator cannot completely consume the H^+ in the solution, resulting in the solution remaining acidic (pH = 4.29). It was shown that the stability of Fe-As species was favored under weakly acidic conditions [52], but Ca-As species dominated the whole encapsulator and Ca-As species were poorly stable under acidic conditions [53]. As a result, the concentration of As in the solution decreased dramatically. The change of As concentration at different pH can be divided into two stages: the first stage in the range of pH from 0 to 1, the As concentration decreases sharply and the final solution is weakly acidic, and the second stage in the range of pH from 1 to 5, the As concentration decreased slowly and the change gradually stabilized and the final solution is alkaline (pH = 10.07~12.19). Therefore, this sequester still has good results in S/S of As at pH > 1.

3.6.2. Effect of Temperature on the Leaching Behavior of As

The pH value was adjusted to 3 with HNO_3, and the ratio of sample to leachate and leaching time were kept constant. The results are shown in Figure 8a, with the increase of temperature, the leaching concentration of As increased from 1.91 µg/L to 24.99 µg/L,

*Int. J. Environ. Res. Public Health* **2022**, *19*, 11247

10 of 14

and the trend of change was stable. The influence of leaching temperature on As leaching concentration is mainly reflected in the change of diffusion coefficient [25], the change of pores and structure of the encapsulator, and the formation and development of hydration products [54]. Leaching is the process by which substances in the solid phase are released into the liquid phase through the surface. The higher the temperature, the faster the diffusion rate of As, which leads to an increase in the concentration of As in the liquid phase. We also found that the amount of change in As concentration per unit temperature decreases as the temperature increases. It was shown that C-S-H and ettringite dissolve at high temperatures [55]. The change in temperature is also reflected in the effect on the pH of the solution; Figure 8b shows the pH value gradually decrease with increasing temperature, which is mainly due to the decrease in the solubility of the hydration product $Ca(OH)_2$ with increasing temperature [56]. The decrease in alkalinity of the solution also affects the stability of the Ca-As species, leading to the release of As from the precipitation.

Figure 8. (**a**) The influence of different temperature on the leaching concentration of As, (**b**) the change of pH after leaching.

3.6.3. SEM Analysis

Figure 9 shows the effect of different pH and temperature on the surface morphology of the encapsulator. These amorphous white substances are mainly C-S-H gels and cementitious materials, and compared to pH = 5 (Figure 9b), at pH = 1 (Figure 9a) it can be observed that the surface is smoother and less dense, and the C-S-H gels and cementitious materials gathered on the surface undergo dissolution, leading to the re-release of the internal As [57]. The dissolution of these materials releases OH^- and raises the pH of the solution, which is consistent with the results in Figure 7. The effect of temperature on the encapsulator is also mainly reflected in the change of C-S-H gel and cementitious materials, compared with 20 °C (Figure 9c), a decrease of C-S-H and cementitious materials aggregated on the surface is clearly observed at 60 °C (Figure 9d). The temperature has a catalytic effect on the chemical reaction, and accelerates the erosive effect of H^+ on C-S-H and cementitious materials [58]. Furthermore, we can observe the appearance of cracks and an increase of surface porosity, where excess heat at higher temperatures can cause thermal damage to the encapsulant. We can observe that cracks appear and the surface pore increase, the excess heat is generated at higher temperatures, thermal damage to the encapsulator can occur.

Int. J. Environ. Res. Public Health **2022**, *19*, 11247

11 of 14
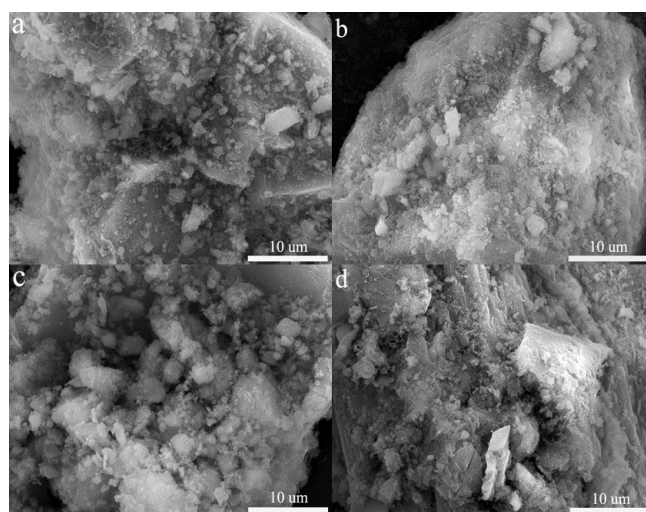
Figure 9. SEM images different pH and temperature: (**a**) pH = 1; (**b**) pH = 5; (**c**) temperature = 20 °C; (**d**) temperature = 60 °C.

3.7. Mechanism of S/S Arsenic

TT is a hazardous solid waste containing As, and if not treated, the internal As will be released into the surrounding environment under the action of natural weathering. The As species in TT are complex, mainly As(III)-S, Fe-As(V), and amorphous As(III)-O species. The As in TT undergoes oxidation reaction, and the As-containing phases As_2S_3 and $Fe(H_2AsO_4)_3 \cdot H_2O$ can be observed in the Figure 2. The reaction conversion mechanism of As is shown in Figure 10. The hydration process of OPC releases OH^-, which results in the whole system being alkaline, and the AsO_4^{3-} released by the $Fe(H_2AsO_4)_3 \cdot H_2O$ reaction combines with Ca^{2+} and OH^- to form $Ca_5(AsO_4)_3(OH)$ and $Ca_3(AsO_4)_2$. A small fraction of Fe^{3+} present in the system can generate $FeAsO_4$ precipitate with AsO_4^{3-}, and also generate $Fe(OH)_3$ colloid with OH^-, but in this system, mainly Ca-As species are still dominant. The solubility of As_2S_3 in water is small, but the hydrolysis products $HAsO_2$ and H_2S can easily react with OH^-, therefore promoting the hydrolysis of As_2S_3. The As_2S_3 and amorphous As(V)-O species provide As(III) and Ca^{2+} to form Ca-As(III) precipitates. Furthermore, the hydration products C-S-H and ettringite also have excellent ability for S/S of As, C-S-H by physical adsorption, ion exchange, and interlayer symbiosis, and ettringite mainly through ion exchange of arsenate group and SO_4^{2-} in the structure. FTIR curves of Si-O, AS-O, and H-O-H indicate that C-S-H and ettringite have ion exchange with As underwent ion exchange in 0. Amorphous C-S-H and needle-tipped ettringite can be clearly observed in 0 and elemental As was also detected by EDS.
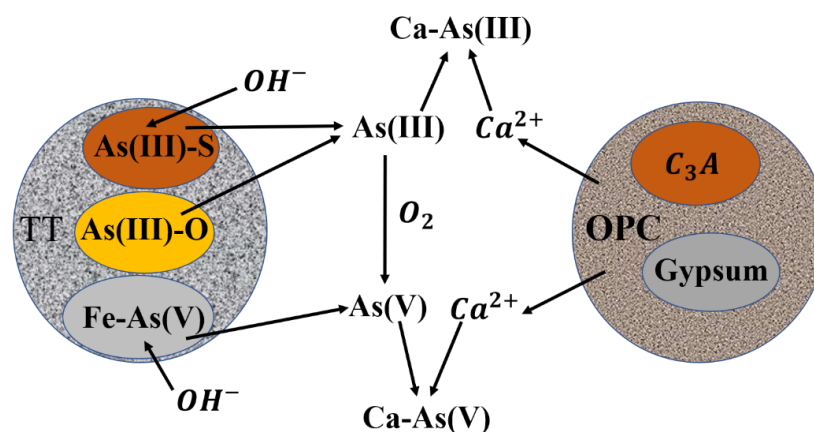
Figure 10. The mechanism of S/S of As in the encapsulator.

The assessment of S/S of As ability should consider the influence of external conditions on the encapsulator. Lowering pH and increasing temperature contribute to the release of As, mainly by promoting the dissolution of As immobilized phase and As immobilized materials, as shown in Figure 9, and pH has a greater effect on As immobilization than temperature. The effects of pH and temperature on the long-term performance of the encapsulator and the effects of other factors on S/S of As need further research. Therefore, it is necessary to employ a systematic and comprehensive assessment of the long-term performance of the encapsulator under various factors in the future to ensure the safety and long-term application of the S/S technology.

4. Conclusions

In this study, S/S treatment of arsenic in TT was performed using OPC and the leaching concentration of arsenic after 28 days was 0.01 mg/L, and it was reduced to a safe range. The leaching concentration of arsenic was reduced to a safe range. During the S/S treatment, OH^- produced by OPC hydration promoted the dissolution of As(III)-S species and Fe-As(V) species and combined with Ca^{2+} to form Ca-As(V) precipitates, and amorphous As(III)-O-containing species also formed Ca-As(III) precipitates with Ca^{2+}, and the dissolved As(III) underwent oxidation reactions, leading to an increase in As(V). The C-S-H gel generated by OPC hydration and ettringite with arsenate group also underwent adsorption and ion exchange to achieve S/S of As effect. In addition, the encapsulator showed good durability in a wide range of acidic environments and temperatures.

Author Contributions: Conceptualization, W.Z. and Z.Z.; data curation, W.Z.; formal analysis, Z.Z.; investigation, W.Z.; methodology, W.Z., Z.Z. and H.Y.; resources, W.Z.; software, W.Z., H.Y., J.W. and C.L.; supervision, Z.Z. and X.Z.; validation, W.Z. and H.Y.; visualization, Z.Z., H.Y., X.Z., J.W. and C.L.; writing—original draft, W.Z.; writing—review and editing, Z.Z., J.W. and C.L. All authors have read and agreed to the published version of the manuscript.

Institutional Review Board Statement: Not applicable.

Informed Consent Statement: Not applicable.

Data Availability Statement: Not applicable.

Conflicts of Interest: The authors declare no conflict of interest.

References

1. Chen, Y.; Xu, J.; Lv, Z.; Xie, R.; Huang, L.; Jiang, J. Impacts of biochar and oyster shells waste on the immobilization of arsenic in highly contaminated soils. *J. Environ. Manag.* **2018**, *217*, 646–653. [CrossRef] [PubMed]
2. Sun, J.; Prommer, H.; Siade, A.J.; Chillrud, S.N.; Mailloux, B.J.; Bostick, B.C. Model-Based Analysis of Arsenic Immobilization via Iron Mineral Transformation under Advective Flows. *Environ. Sci. Technol.* **2018**, *52*, 9243–9253. [CrossRef] [PubMed]
3. Nazari, A.M.; Radzinski, R.; Ghahreman, A. Review of arsenic metallurgy: Treatment of arsenical minerals and the immobilization of arsenic. *Hydrometallurgy* **2017**, *174*, 258–281. [CrossRef]
4. Yoshiasa, A.; Tokuda, M.; Misawa, M.; Shimojo, F.; Momma, K.; Miyawaki, R.; Matsubara, S.; Nakatsuka, A.; Sugiyama, K. Natural arsenic with a unique order structure: Potential for new quantum materials. *Sci. Rep.* **2019**, *9*, 6275. [CrossRef]
5. Shamsudduha, M.; Uddin, A.; Saunders, J.A.; Lee, M.-K. Quaternary stratigraphy, sediment characteristics and geochemistry of arsenic-contaminated alluvial aquifers in the Ganges-Brahmaputra floodplain in central Bangladesh. *J. Contam. Hydrol.* **2008**, *99*, 112–136. [CrossRef]
6. Wen, Z.; Zhang, Y.; Zhou, X.; Chen, R. Effective As(III) and As(V) immobilization from aqueous solution by nascent ferrous hydroxide colloids (FHC). *Sep. Purif. Technol.* **2017**, *176*, 395–401. [CrossRef]
7. Silva, R.A.; Park, J.; Ilyas, S.; Borja, D.; Zhao, H.; Urík, M.; Rastegar, S.O.; Kim, H. Biodegradation mechanism of arsenopyrite mine tailing with Acidithiobacillus ferrooxidans and influence of ferric supplements. *Int. Biodeterior. Biodegrad.* **2020**, *153*, 105042. [CrossRef]
8. Wang, X.; Ding, J.; Wang, L.; Zhang, S.; Hou, H.; Zhang, J.; Chen, J.; Ma, M.; Tsang, D.C.W.; Wu, X. Stabilization treatment of arsenic-alkali residue (AAR): Effect of the coexisting soluble carbonate on arsenic stabilization. *Environ. Int.* **2020**, *135*, 105406. [CrossRef]

9. Wang, X.; Zhang, H.; Wang, L.; Chen, J.; Xu, S.; Hou, H.; Shi, Y.; Zhang, J.; Ma, M.; Tsang, D.C.W.; et al. Transformation of arsenic during realgar tailings stabilization using ferrous sulfate in a pilot-scale treatment. *Sci. Total Environ.* **2019**, *668*, 32–39. [CrossRef]
10. Vermeulen, M.; Sanyova, J.; Janssens, K.; Nuyts, G.; De Meyer, S.; De Wael, K. The darkening of copper- or lead-based pigments explained by a structural modification of natural orpiment: A spectroscopic and electrochemical study. *J. Anal. At. Spectrom.* **2017**, *32*, 1331–1341. [CrossRef]
11. Alvarez-Ayuso, E.; Murciego, A. Stabilization methods for the treatment of weathered arsenopyrite mine wastes: Arsenic immobilization under selective leaching conditions. *J. Clean. Prod.* **2021**, *283*, 125265. [CrossRef]
12. Hammond, C.M.; Root, R.A.; Maier, R.M.; Chorover, J. Mechanisms of Arsenic Sequestration by Prosopis juliflora during the Phytostabilization of Metalliferous Mine Tailings. *Environ. Sci. Technol.* **2018**, *52*, 1156–1164. [CrossRef] [PubMed]
13. Hamberg, R.; Maurice, C.; Alakangas, L. The use of low binder proportions in cemented paste backfill—Effects on As-leaching. *Miner. Eng.* **2015**, *78*, 74–82. [CrossRef]
14. Zhang, Y.; Gao, W.; Ni, W.; Zhang, S.; Li, Y.; Wang, K.; Huang, X.; Fu, P.; Hu, W. Influence of calcium hydroxide addition on arsenic leaching and solidification/stabilisation behaviour of metallurgical-slag-based green mining fill. *J. Hazard. Mater.* **2020**, *390*, 122161. [CrossRef]
15. Wang, J.; Sun, X.; Xing, Y.; Xia, J.; Feng, X. Immobilization of mercury and arsenic in a mine tailing from a typical Carlin-type gold mining site in southwestern part of China. *J. Clean. Prod.* **2019**, *240*, 118171. [CrossRef]
16. Zhang, Y.; Zhang, S.; Ni, W.; Yan, Q.; Gao, W.; Li, Y. Immobilisation of high-arsenic-containing tailings by using metallurgical slag-cementing materials. *Chemosphere* **2019**, *223*, 117–123. [CrossRef]
17. Long, W.J.; Ye, T.H.; Xing, F.; Khayat, K.H. Decalcification effect on stabilization/solidification performance of Pb-containing geopolymers. *Cem. Concr. Compos.* **2020**, *114*, 103803. [CrossRef]
18. Wang, L.; Chen, L.; Tsang, D.C.W.; Zhou, Y.; Rinklebe, J.; Song, H.; Kwon, E.E.; Baek, K.; Ok, Y.S. Mechanistic insights into red mud, blast furnace slag, or metakaolin-assisted stabilization/solidification of arsenic-contaminated sediment. *Environ. Int.* **2019**, *133*, 105247. [CrossRef] [PubMed]
19. Wang, L.; Yu, K.; Li, J.-S.; Tsang, D.C.W.; Poon, C.S.; Yoo, J.-C.; Baek, K.; Ding, S.; Hou, D.; Dai, J.-G. Low-carbon and low-alkalinity stabilization/solidification of high-Pb contaminated soil. *Chem. Eng. J.* **2018**, *351*, 418–427. [CrossRef]
20. Wang, L.; Cho, D.W.; Tsang, D.C.W.; Cao, X.; Hou, D.; Shen, Z.; Alessi, D.S.; Ok, Y.S.; Poon, C.S. Green remediation of As and Pb contaminated soil using cement-free clay-based stabilization/solidification. *Environ. Int.* **2019**, *126*, 336–345. [CrossRef]
21. Liu, D.G.; Min, X.B.; Ke, Y.; Chai, L.-Y.; Liang, Y.; Li, Y.; Yao, L.; Wang, Z. Co-treatment of flotation waste, neutralization sludge, and arsenic-containing gypsum sludge from copper smelting: Solidification/stabilization of arsenic and heavy metals with minimal cement clinker. *Environ. Sci. Pollut. Res.* **2018**, *25*, 7600–7607. [CrossRef] [PubMed]
22. Kunther, W.; Lothenbach, B.; Skibsted, J. Influence of the Ca/Si ratio of the C-S-H phase on the interaction with sulfate ions and its impact on the ettringite crystallization pressure. *Cem. Concr. Res.* **2015**, *69*, 37–49. [CrossRef]
23. Sasaki, T.; Iizuka, A.; Watanabe, M.; Hongo, T.; Yamasaki, A. Preparation and performance of arsenate (V) adsorbents derived from concrete wastes. *Waste Manag.* **2014**, *34*, 1829–1835. [CrossRef] [PubMed]
24. Zhu, Y.; Wei, W.; Tang, S.; Zhu, Z.; Yan, Q.; Zhang, L.; Deng, H. A comparative study on the dissolution and stability of beudantite and hidalgoite at pH 2–12 and 25–45 degrees C for the possible long-term simultaneous immobilization of arsenic and lead. *Chemosphere* **2021**, *263*, 128386.
25. Bull, A.J.; Fall, M. Curing temperature dependency of the release of arsenic from cemented paste backfill made with Portland cement. *J. Environ. Manag.* **2020**, *269*, 110772. [CrossRef]
26. Zhu, J.; Zhang, P.; Yuan, S.; Tong, M. Arsenic oxidation and immobilization in acid mine drainage in karst areas. *Sci. Total Environ.* **2020**, *727*, 138629. [CrossRef]
27. Yang, D.Z.; Sasaki, A.; Endo, M. Reclamation of an arsenic-bearing gypsum via acid washing and CaO-As stabilization involving svabite formation in thermal treatment. *J. Environ. Manag.* **2019**, *231*, 811–818. [CrossRef]
28. Ghosh, A.; Mukiibi, M.; Ela, W. TCLP underestimates leaching of arsenic from solid residuals under landfill conditions. *Environ. Sci. Technol.* **2004**, *38*, 4677–4682. [CrossRef]
29. Wang, C.; Hu, X.; Chen, M.L.; Wu, Y.H. Total concentrations and fractions of Cd, Cr, Pb, Cu, Ni and Zn in sewage sludge from municipal and industrial wastewater treatment plants. *J. Hazard. Mater.* **2005**, *119*, 245–249. [CrossRef]
30. Ji, Z.H.; Pei, Y.S. Immobilization efficiency and mechanism of metal cations (Cd^{2+}, Pb^{2+} and Zn^{2+}) and anions (AsO_4^{3-} and $Cr_2O_7^{2-}$) in wastes-based geopolymer. *J. Hazard. Mater.* **2020**, *384*, 121290. [CrossRef] [PubMed]
31. Li, Y.; Min, X.; Ke, Y.; Fei, J.; Liu, D.; Tang, C. Immobilization potential and immobilization mechanism of arsenic in cemented paste backfill. *Miner. Eng.* **2019**, *138*, 101–107. [CrossRef]
32. Askarian, M.; Tao, Z.; Samali, B.; Adam, G.; Shuaibu, R. Mix composition and characterisation of one-part geopolymers with different activators. *Constr. Build. Mater.* **2019**, *225*, 526–537. [CrossRef]
33. Min, X.; Liu, D.; Chai, L.; Ke, Y.; Liang, Y.; Shi, M.; Li, Y.; Yang, C.; Wang, W.; Wang, Z. Comparison of arsenic immobilization properties among calcium silicate hydrate, ettringite, and friedel's salt in a slag-based binder. *Environ. Prog. Sustain. Energy* **2019**, *38*, S422–S428. [CrossRef]
34. Kim, B.J.; Jang, J.G.; Park, C.Y.; Han, O.H.; Kim, H.K. Recycling of arsenic-rich mine tailings in controlled low-strength materials. *J. Clean. Prod.* **2016**, *118*, 151–161. [CrossRef]

Int. J. Environ. Res. Public Health **2022**, *19*, 11247

14 of 14

35. Li, Y.; Min, X.; Ke, Y.; Chai, L.; Shi, M.; Tang, C.; Wang, Q.; Liang, Y.; Lei, J.; Liu, D. Utilization of red mud and Pb/Zn smelter waste for the synthesis of a red mud-based cementitious material. *J. Hazard. Mater.* **2018**, *344*, 343–349. [CrossRef] [PubMed]

36. Zhang, J.; Tan, H.; He, X.; Yang, W.; Deng, X.; Su, Y.; Yang, J. Compressive strength and hydration process of ground granulated blast furnace slag-waste gypsum system managed by wet grinding. *Constr. Build. Mater.* **2019**, *228*, UNSP116777. [CrossRef]

37. Lu, Q.; Xiao, H.; Du, Y.; Du, D. Using CaO to stabilize arsenic sulfide slag by moderate temperature calcination. *Environ. Earth Sci.* **2017**, *76*, 262. [CrossRef]

38. Kurz, E.E.C.; Luong, V.T.; Hellriegel, U.; Leidinger, F.; Luu, T.L.; Bundsch, J.; Hoinkis, J. Iron-based subsurface arsenic removal (SAR): Results of a long-term pilot-scale test in Vietnam. *Water Res.* **2020**, *181*, 115929. [CrossRef]

39. Zhong, D.; Zhao, Z.; Jiang, Y.; Yang, X.; Wang, L.; Chen, J.; Guan, C.; Zhang, Y.; Tsang, D.C.W.; Crittenden, J.C. Contrasting abiotic As(III) immobilization by undissolved and dissolved fractions of biochar in Ca2+-rich groundwater under anoxic conditions. *Water Res.* **2020**, *183*, 116106. [CrossRef]

40. Elyamine, A.M.; Moussa, M.G.; Afzal, J.; Rana, M.S.; Imran, M.; Zhao, X.; Hu, C.X. Modified Rice Straw Enhanced Cadmium (II) Immobilization in Soil and Promoted the Degradation of Phenanthrene in Co-Contaminated Soil. *Int. J. Mol. Sci.* **2019**, *20*, 2189. [CrossRef]

41. Zhang, M.; Yang, C.; Zhao, M.; Yang, K.; Shen, R.; Zheng, Y. Immobilization potential of Cr(VI) in sodium hydroxide activated slag pastes. *J. Hazard. Mater.* **2017**, *321*, 281–289. [CrossRef] [PubMed]

42. Liu, J.; Hu, L.; Tang, L.; Ren, J. Utilisation of municipal solid waste incinerator (MSWI) fl y ash with metakaolin for preparation of alkali-activated cementitious material. *J. Hazard. Mater.* **2021**, *402*, 123451. [CrossRef] [PubMed]

43. Ramesh, S.; Yuen, T.F.; Shen, C.J. Conductivity and FTIR studies on PEO-LiX X: CF3SO3-, SO42- polymer electrolytes. *Spectrochim. Acta Part A Mol. Biomol. Spectrosc.* **2008**, *69*, 670–675. [CrossRef] [PubMed]

44. El-Moselhy, M.M.; Ates, A.; Celebi, A. Synthesis and characterization of hybrid iron oxide silicates for selective removal of arsenic oxyanions from contaminated water. *J. Colloid Interface Sci.* **2017**, *488*, 335–347. [CrossRef]

45. Zhang, D.; Chen, H.; Xia, J.; Nie, Z.; Fan, X.; Liu, H.; Zheng, L.; Zhang, L.; Yang, H. Humic acid promotes arsenopyrite bio-oxidation and arsenic immobilization. *J. Hazard. Mater.* **2020**, *384*, 121359. [CrossRef]

46. Tabelin, C.B.; Corpuz, R.D.; Iarashi, T.; Villacorte-Tabeline, M.; Ito, M.; Hiroyoshi, N. Hematite-catalysed scorodite formation as a novel arsenic immobilisation strategy under ambient conditions. *Chemosphere* **2019**, *233*, 946–953. [CrossRef]

47. Zhao, Z.; Song, Y.; Min, X.; Liang, Y.; Chai, L.; Shi, M. XPS and FTIR studies of sodium arsenate vitrification by cullet. *J. Non-Cryst. Solids* **2018**, *502*, 254. [CrossRef]

48. Opiso, E.M.; Tabelin, C.B.; Maestre, C.V.; Aseniero, J.P.J.; Park, I.; Villacorte-Tabelin, M. Synthesis and characterization of coal fly ash and palm oil fuel ash modified artisanal and small-scale gold mine (ASGM) tailings based geopolymer using sugar mill lime sludge as Ca-based activator. *Heliyon* **2021**, *7*, e06654. [CrossRef]

49. Suess, E.; Planer-Friedrich, B. Thioarsenate formation upon dissolution of orpiment and arsenopyrite. *Chemosphere* **2012**, *89*, 1390–1398. [CrossRef]

50. Phenrat, T.; Marhaba, T.F.; Rachakornkij, M. A SEM and X-ray study for investigation of solidified/stabilized arsenic-iron hydroxide sludge. *J. Hazard. Mater.* **2005**, *118*, 185–195. [CrossRef]

51. Fei, J.; Ma, J.; Yang, J.; Liang, Y.; Ke, Y.; Yao, L.; Li, Y.; Liu, D.; Min, X. Effect of simulated acid rain on stability of arsenic calcium residue in residue field. *Environ. Geochem. Health* **2020**, *42*, 769–780. [CrossRef] [PubMed]

52. Wang, S.; Zhang, D.; Li, X.; Zhang, G.; Wang, Y.; Wang, X.; Gomez, M.A.; Jia, Y. Arsenic associated with gypsum produced from Fe(III)-As(V) coprecipitation: Implications for the stability of industrial As-bearing waste. *J. Hazard. Mater.* **2018**, *360*, 311–318. [CrossRef] [PubMed]

53. Ma, X.; Yao, S.; Yuan, Z.; Bi, R.; Wu, X.; Zhang, J.; Wang, S.; Wang, X.; Jia, Y. Detoxification and reclamation of hydrometallurgical arsenic- and trace metals-bearing gypsum via hydrothermal recrystallization in acid solution. *Chemosphere* **2020**, *250*, 126290. [CrossRef]

54. Zhang, W.; Zhao, L.; Mccabe, B.A.; Chen, Y.; Morrison, L. Dredged marine sediments stabilized/solidi fied with cement and GGBS: Factors affecting mechanical behaviour and leachability. *Sci. Total Environ.* **2020**, *733*, 138551. [CrossRef]

55. Wang, P.; Mo, R.; Li, S.; Xu, J.; Jin, Z.; Zhao, T.; Wang, D. A chemo-damage-transport model for chloride ions diffusion n cement-based materials: Combined effects of sulfate attack and temperature. *Constr. Build. Mater.* **2021**, *288*, 123121. [CrossRef]

56. Gacsi, A.; Kutus, B.; Konya, Z.; Kukovecz, A.; Pálinkó, I.; Sipos, P. Estimation of the solubility product of hydrocalumite-hydroxide, a layered double hydroxide with the formula of $Ca_2Al(OH)_6OH \cdot nH_2O$. *J. Phys. Chem. Solids* **2016**, *98*, 167–173. [CrossRef]

57. Li, G.; Li, X.; Qi, X.; Zhang, A. Copper slag gel encapsulates sludge through encapsulation and precipitation in weakly acidic to strongly basic environments. *J. Clean. Prod.* **2021**, *294*, 126227. [CrossRef]

58. Bull, A.J.; Fall, M. Thermally induced changes in metalloid leachability of cemented paste backfill that contains blast furnace slag. *Miner. Eng.* **2020**, *156*, 106520. [CrossRef]